Journal of Building Engineering

SELF-HEALING OF SLAG-CEMENT ULTRA-HIGH PERFORMANCE STEEL FIBER REINFORCED CONCRETE (UHPFRC) CONTAINING SISAL FIBERS AS HEALING CONVEYOR

--Manuscript Draft--

Manuscript Number:	
Article Type:	Research Paper
Section/Category:	Building materials
Keywords:	self-healing; sisal fiber; slag-cement ultra-high performance concrete; tensile cracking
Corresponding Author:	Romildo Toledo Filho COPPE, Universidade Federal do Rio de Janeiro Rio de Janeiro, Brazil
First Author:	Tamara Nunes da Cunha Moreira
Order of Authors:	Tamara Nunes da Cunha Moreira
	Romildo Toledo Filho
	Visar Krelani
	Saulo Rocha Ferreira
	Liberato Ferrara
Abstract:	This paper presents the research on the influence of sisal fibers on the self-healing capacity of slag-cement UHPFRC reinforced with steel fibers. In order to evaluate the composite healing capacity, specimens were submitted to pre-cracking by tensile test and then to a 3 months of wetting and drying cycles treatment. Treated specimens were resubmitted to tensile test and evaluated by Optical and Electronic microscopy and CT Scan. Results indicate that the sisal fiber works as a healing conveyor improving by about 20% and 15% the tensile stress and post cracking energy of treated specimens, respectively. Sisal fibers played a major role densifying the interface, working as a vehicle for the healing agents into small interface cracks. All specimens with cracks under 80 μm could completely self-seal mainly by calcium carbonate. Wider cracks could not be completely sealed, though the specimens exhibited a recovery of the mechanical behavior essentially due to late slag-cement hydration.
Suggested Reviewers:	Edward Koenders Darmstadt University of Technology: Technische Universitat Darmstadt e.a.b.koenders@tudelft.nl High profile researcher with major experience in the material science field
	Marco Di Prisco POLIMI: Politecnico di Milano marco.diprisco@polimi.it One of the best researchers in the fracture area
Opposed Reviewers:	

Journal of Building Engineering
ELSEVIER

Subject: Manuscript submission of a research article proposed for publication on "*Journal of Building Engineering*"

Dear Editors-in-Chief,

It is my pleasure to propose the manuscript entitled "***SELF-HEALING OF SLAG-CEMENT ULTRA-HIGH PERFORMANCE STEEL FIBER REINFORCED CONCRETE (UHPFRC) CONTAINING SISAL FIBERS AS HEALING CONVEYOR*** " co-authored by Tamara Nunes, Visar Krelani, Saulo Rocha Ferreira, Liberato Ferrara and myself, for possible publication on the Journal of Building Engineering.

This study proposes an analysis of the influence of sisal fibers on the self-healing capacity of slag-cement UHPFRC reinforced with steel fibers. Mechanical and chemical performance is pursued through TGA and tensile tests. Two mixes were analyzed one with and other without sisal insertion. Moreover, as the modern concrete design requires sustainability allied with performance, a slag-cement self-healing concrete were developed. This study also demonstrates that the sisal fibers can be considered as healing conveyors that are capable of nucleation of calcium carbonate bridging the crack increasing the mechanical performance of the studied specimens.

I hope that this work will meet the interest/scope of the Journal of Building Engineering and can be considered for the revision process.

Best regards,

Prof. Romildo D. Toledo Filho
Civil Engineering Program-COPPE
Universidade Federal do Rio de Janeiro - Brazil

Highlights

- Environmental friendly ultra-high performance concrete made with blast furnace slag and cement proved to reach high tensile and compressive tension
- Self-healing occurs due to late hydration of anhydrous cement and development of calcium carbonate
- Sisal’s fibers work as a conveyor for late hydration as well as calcium carbonate nucleation
- Vegetable fibers enhance the self-healing phenomenon

SELF-HEALING OF SLAG-CEMENT ULTRA-HIGH PERFORMANCE STEEL FIBER REINFORCED CONCRETE (UHPFRC) CONTAINING SISAL FIBERS AS HEALING CONVEYOR

Tamara Nunes da C. Moreira[a], Visar Krelani[b], Saulo Rocha Ferreira[c], Liberato Ferrara[d], Romildo Dias Toledo Filho[e,*]

[a,e] Civil Engineering Program, COPPE/UFRJ, Rio de Janeiro, RJ, Brazil
[b] Civil Engineering and Infrastructure Department, University for Business and Technology UBT, Pristina, Kosova
[c] Civil Engineering Department, Federal University of Lavras, Lavras, MG, Brazil
[d] Department of Civil and Environmental Engineering, Politecnico di Milano, Italy

ABSTRACT

This paper presents the research on the influence of sisal fibers on the self-healing capacity of slag-cement UHPFRC reinforced with steel fibers. In order to evaluate the composite healing capacity, specimens were submitted to pre-cracking by tensile test and then to a 3 months of wetting and drying cycles treatment. Treated specimens were resubmitted to tensile test and evaluated by Optical and Electronic microscopy and CT Scan. Results indicate that the sisal fiber works as a healing conveyor improving by about 20% and 15% the tensile stress and post cracking energy of treated specimens, respectively. Sisal fibers played a major role densifying the interface, working as a vehicle for the healing agents into small interface cracks. All specimens with cracks under 80 μm could completely self-seal mainly by calcium carbonate. Wider cracks could not be completely sealed, though the specimens exhibited a recovery of the mechanical behavior essentially due to late slag-cement hydration.

KEYWORDS: self-healing, sisal fiber, steel fiber, ultra-high performance concrete, slag-cement, tensile cracking.

[*]Corresponding author
Romildo Dias Toledo Filho
e-mail: toledo@coc.ufrj.br
COPPE/UFRJ
Technology Center, I - 116 - NUMATS
C.P. 68506
ZIP CODE: 21941-972 - Rio de Janeiro - RJ
Brazil

1. INTRODUCTION

Self-healing of concrete can be defined as the ability of concrete to repair its cracks autogenously or autonomously, i.e. thanks to its own conventional constituents or to tailored additions, but in any case without any external intervention [1] [2] [3]. According to De Belie et al [4] there are four basic mechanisms for self-healing to occur. The first one consists in precipitation of calcium carbonate at the crack surface, the second by dirty water and concrete particles blocking the crack; the third is through late hydration of cementitious materials that remains un-hydrated and the last one relies on C-S-H expansion. The first and third types are identified in the literature as the main causes of self-healing in concrete. Nevertheless, autogenous healing has its limitation, since, for example it needs humidity in order to enhance the calcium carbonate precipitation reaction, as well as the C-S-H formation one. The size of calcium carbonate crystals varies, depending on the environment, ranging between 0.2 and 30 microns, which may also affect the crack opening limit for sealing. [5] [6]

In order to improve autogenous self-healing on cement based materials several "stimulating" or autonomous healing techniques have been developed, e.g. employing mineral and/or chemical additions, polymeric and biological agents respectively.

Krelani and Ferrara et al [7] [8] performed a partial substitution of the cement content for blast furnace slag in order to enhance the autonomous healing and in an attempt to enhance the environmental sustainability of the matrix. Blast-furnace slag was chosen due its slow hydration property, therefore, capable of promoting healing in mature concretes. According to Mehta and Monteiro [9], finely ground blast-furnace slag is a nonmetallic self-cementing product consisting essentially of calcium silicates and alumino-silicates and other bases that contribute to enhance concrete performance in at least three aspects. The first is the slow reaction of the slag; which means that the rates of hydration heat released, but of strength development as well, will also be slow. Secondly, the reaction is lime-consuming instead of lime-producing. And the third, the pozzolanic and late hydration reaction of the slag contributes to refine pore size, filling up the capillary spaces, which improves durability and crack control.

Autogenous healing can be also stimulated by means of constituents which act as catalyst of the aforementioned self-healing mechanisms, including, e.g., crystalline admixtures, whose healing stimulation mechanisms have been recently reviewed in detail [10]. The effectiveness has been widely assessed with reference to a broad variety of cementitious composites, ranging from normal strength concrete to Ultra High Performance (Fiber Reinforced Concrete (UHPC/UHPFRC) [8] [11] and including effects of repeated cracking and healing cycles [12] as well as of aggressive environments.

Among the autonomous healing techniques, polymer encapsulation, with both micro- and macro-capsules, vascular-based methods, electrodeposition, methods relying upon microbial activity, in case employing capsules as carriers and protectors of bacteria, and self-healing method through embedding shape memory alloys (SMAs) have been reported, with different levels of efficacy [13] [14] [15] [1].

There are different ways to induce a crack in order to study self-healing in cement based materials [16]. Crack induction by bending tests is actually the most commonly reported method

in the literature. In the case of UHPC/UHPFRCs a 4-point bending test is preferred, resulting, in the central constant bending moment zone of the specimen, into multiple thinly opened cracks which can be easier healed [17]. Crack induction by tensile tests has been more rarely employed due to laboratory challenges, though; concerning the pretended phenomenon to be studied, a method using one single and clearly defined crack enhances the self-healing to its maximum performance [7] and allows a clearer quantification of it. This is of the most importance, considering the achievement of a consensus on the quantification of sealing and healing as well as on the limit crack width/opening that can be sealed, depending on the used self-healing stimulating/triggering additions as well as on the healing and structural service scenario [18].

Although a huge effort has been made on concept, formulation and validation of different stimulated autogenous and autonomous self-healing technologies, some of them, especially the autonomous ones, are still in embryonic stage of development and scant information exist mainly on the environmental sustainability and economic viability of their production and incorporation into real scale structures made of/retrofitted with self-healing cement based materials [19]. Therefore, there is a practical gap that needs to be filled involving the economy viability and cost/benefit of the self-healing structures on construction sites.

In this respect, the incorporation of vegetal fibers into a cementitious matrix as healing conveyor has an enormous advantage. The cost of vegetal fibers is very low and they usually require just a wash in hot water to be incorporated into the concrete mix. These types of fiber have a porous hierarchical structure. The structure is formed by several different wall layers (each one with a singular chemical composition). The porous size on those structure ranges between 0.2 nm to 30 nm and until 8 μm form lumen size [22]. This variable porous media promotes a high and fast water absorption followed by a slow and controlled desorption process [23]. The absorption happens during the molding process, interaction with the water from the mix design. The desorption is triggered off by several phenomena such as temperature elevation, matrix water evaporation, matrix necessities (more water for hydration reactions), etc [24][25]. In resume, the water removal from sisal fibers is ruled by the moisture equilibrium in the system. The porous fiber system also works as a network for water to percolate inside the concrete specimen, to trigger off and stimulate the delayed hydration and carbonation phenomena which are responsible of the self-healing processes, and also feature selective attraction for metallic ions, especially calcium.

This research aims to combine, in Ultra High Performance steel FRC, stimulated autogenous healing through mineral additions, as favored by the mix composition which features high binder content and low water/binder ratio with vegetal fibers. With the aim to reduce the environmental footprint of UHPFRC, part of the cement (50% by volume) was substituted with blast furnace slag, in analogy with previously reported investigations [26] [27]. Straight steel fibers were added, at a volume fraction equal to 1.28%, conducive to an easier and more effective self-healing, and also resulting into deflection hardening and moderate strain hardening behavior. Steel fibers were used in combination with 0.28% by volume of sisal fibers, acting as carriers of the water, which is the main healing agent in all autogenous and most autonomous healing processes in cement based materials, as well as nucleation spots for calcium carbonate deposition, thanks to their ability to maintain a highly moist micro-environment.

In order to validate the effectiveness of the proposed idea, rectangular specimens with a notch

were cast, pre-cracked through direct tensile test, submitted to wetting and drying cycles and retested through the same tensile test set-up (Figure 1), in order to assess the effectiveness of the achieved healing through recovery, if any, of the tensile load bearing, deformation and energy dissipation capacity.

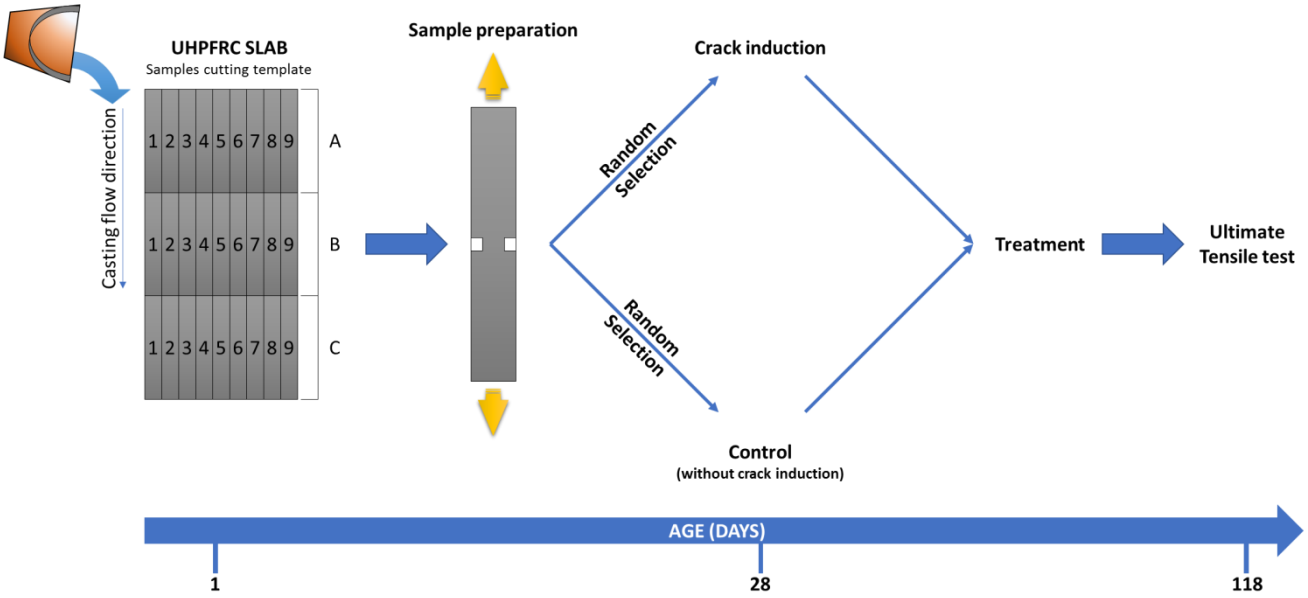

Figure 1. Schematic description of the stages of the research program: direction of the slab concrete casting, sample preparation, random selection for control and crack induction samples at 28 days, treatment period and tensile test to failure after treatment

2. METHODS AND MATERIALS

2.1 Materials

The investigated cementitious composites composition is reported in Table 1, contain Brazilian cement CPV ARI Maxx supplied by Lafarge/Holcim (correspondent to ASTM-C150, Type I).

Table 1
Mix design and healing treatment time for all studied composites

Mix design	Materials (kg/m³)							
	Cement	Fine Aggregate	Blast Furnace Slag	Water	Sisal Fiber	Steel Fiber	Healing Treatment	Compressive Stress [MPa]
S1.28	600	980	500	200	-	100	3 m	103.3±3.5
S1.28Si0.28	600	980	500	200	3	100	3 m	111.1±2.3

This cement has a particle size between 0,2-200 μm, superficial area of 1,03 μm² and density of 3,16 g/cm³. Blast furnace slag from Brazil's National Steel Company was also used in the mix, presenting particle size between 0,3-200 μm, superficial area of 1,17 μm² and density of 2,98

g/cm³ - chemical composition is reported in Table 2.

Table 2
Blast furnace slag chemical composition

Compound	Composition (%)
CaO	48.00
SiO_2	29.02
Al_2O_3	12.86
MgO	5.12
SO3	2.58
MnO	0.67
TiO_2	0.52
K_2O	0.51
Fe_2O_3	0.35
BaO	0.18
SrO	0.14
ZrO_2	0.05
Y_2O_3	0.01

Washed river sand with a maximum diameter of 2 mm, water and a polycarboxylate superplasticizer (SP) - Glenium 51 - manufactured by BASF were used to complete the concrete mix. In order to reinforce and provide self-healing features, two types of fibers were used: steel fibers with a nominal length of 13 mm and nominal diameter 0.16 mm supplied by BEKAERT (DRAMIX OL 13/.16) and vegetal sisal fibers by APAEB Company, Brazil. According to [22] sisal fibers present around 500 MPa with an average area of 0.023 (±0.007) mm², a density of 1,1 g/cm³, initial humidity of 12% and water absorption capacity of 246%, according to [23]. In order to remove the mucilage and greases, sisal fibers were heated from 21 to 80 ºC in tap water, kept at the maximum temperature for two hours and then submitted to a natural cooling process, avoiding thermal shock, followed by washing in running tap water. After treatment the long fibers were dried at room temperature (21º C), combed and cut to a nominal size of 13 mm.

The water/binder ratio of the investigated concretes was set to 0.18 which leads to a supposed high number of un-hydrated binder grains, enhancing the autogenous healing. Two mixes were cast. The first mix (S1.28) contained 1.28% by volume of steel fibers and no sisal fibers. The second one (S1.28Si0.28) contained also 1.28% by volume of steel fibers and 0.28% of sisal fibers. As remarked above, the sisal fibers were added in order to promote better moisture dispersion on the matrix, working as healing carrier agent.

2.2. Mix procedure, casting and curing conditions

The concrete mixtures were batched using a 50 L Eximea Machines ® planetary mixer in a room with controlled temperature (21 ± 1°C). In order to produce the UHPFRC, first the cement and slag were dry mixed for 2 minutes for homogenization. Water and superplasticizer were then

poured into the mixture during 2 further minutes and then the paste was mixed for 8 minutes. The sand was then added and the mortar was mixed for another 8 minutes until it became homogenous. The final procedure consisted of the addition of steel and, in case, sisal fibers, after which mixing was continued for 5 more minutes to obtain the required self-compacting consistency of the UHPFRC.

A slab 600 mm wide x 900 mm long and 30 mm thick was cast by pouring the mix from the planetary mixer barrel at one short side in order to provide a continuous flow and thus guiding most of the fibers parallel to the slab longitudinal direction (see Figure 2(a)). 24 hours after casting, the slab was demolded and placed into a fog room (RH ≥95%) to be moist cured for 28 days.

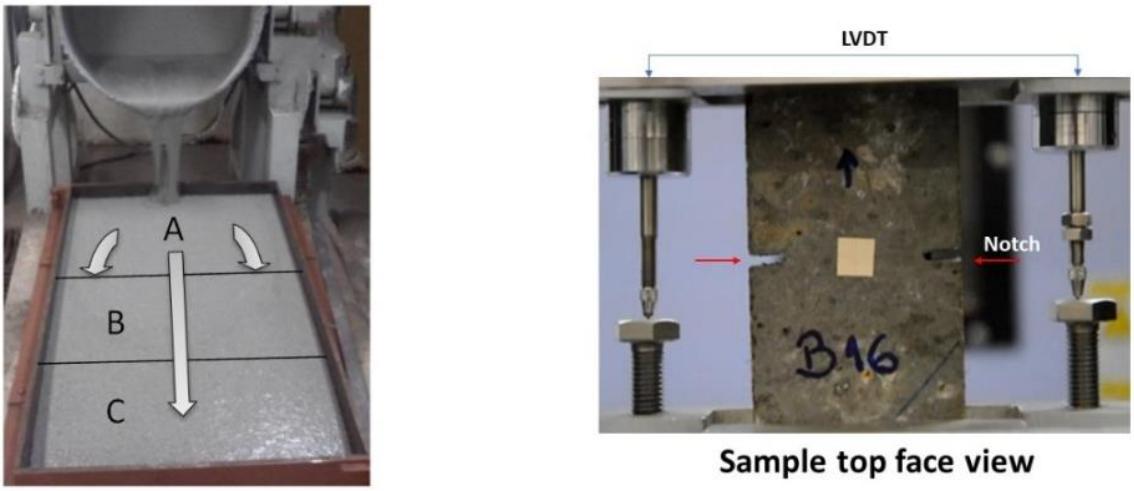

(a) (b)

Figure 2. Sample preparation and test setup: (a) casting procedure; (b) tensile test setup for crack induction and failure

2.2.1. Specimen preparation

The slab was cut into 27 specimens (300 x 55 x 30 mm) which then were crack induced through direct tensile tests. In order to concentrate stresses and promote the opening of one single crack, for easier control and assessment of the healing process, a 10 mm deep notch was cut on either side in the middle zone of the specimen.

Three samples were randomly chosen for crack induction for each mixture and 2 other specimens were also randomly chosen for control. The control specimens do not have cracks but were submitted to the same wet and dry (W&D) cycles, as the cracked specimens.

2.3. Self-healing evaluation

2.3.1. Crack induction

Crack induction was performed at 28 days through direct tensile test. It is important to highlight that the 28 days age was chosen in order to ensure a high cement hydration before any crack induction. The crack was induced in the specimens by means of displacement-controlled tensile test performed using a Universal Machine - Shimadzu 300 kN and at a displacement rate equal to 0.1mm/min. The test was carried out until a crack opening of 0.2 mm was reached. The crack opening was controlled by means of two LVDTs placed aside of the specimen (see Figure 2(b)).

2.3.2. Treatment and tensile tests to failure

After crack induction, the specimens were submitted to wetting and drying cycles treatment [24h/24h] during 3 months. The treatment was performed in a tap water reservoir in a room with controlled temperature and humidity (21±1ºC and 65±3%). Un-cracked control samples were also submitted to the same exposure conditions.
After 3 months, of wetting and drying cycles, the specimens were submitted to ultimate direct tensile test until final collapse. The control samples were also tested until failure, using the same method described at item 2.3.1.

2.4. Mechanical recovery Index

In order to evaluate the mechanical behavior after treatment two indexes were defined and calculated: Index of Damage Recovery (IDR) and Index of Tension Recovery (ITR). For the last one, two different definitions are proposed, resulting in two alternative indexes, respectively ITR_1 and ITR_2 (Figure 3(a)).

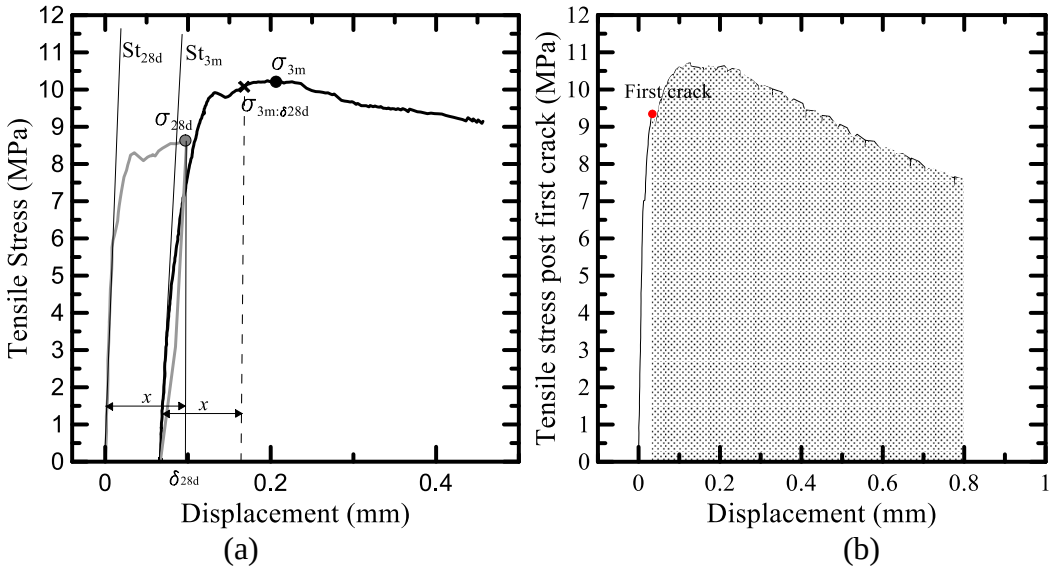

Figure 3. Graphic explanation of developed indexes on a Tensile Stress x Displacement graph (a) ITR1 and ITR2 (b) post first crack energy

The Index of Damage Recovery was calculated dividing the specimen stiffness as inferred from after treatment test results (St_{3m}) by the specimen stiffness as measured before treatment (St_{28d}).

$$IDR = \frac{St_{3m}}{St_{28d}} \quad \text{(eq.1)}$$

ITR_1 was calculated dividing the maximum tensile stress attained in the failure tensile test performed after treatment (σ_{3m}) by the maximum tensile stress reached during the crack induction test at 28 days (σ_{28d}).

$$ITR_1 = \frac{\sigma_{3m}}{\sigma_{28d}} \quad \text{(eq.2)}$$

Finally, ITR_2 was calculated dividing the after treatment tensile stress corresponding to the

maximum displacement reached during crack induction ($\sigma_{3m:\delta 28d}$) by the maximum tensile stress at the 28 days age test (σ_{28d}).

$$ITR_2 = \frac{\sigma_{3m:\delta 28d}}{\sigma_{28d}} \quad \text{(eq.3)}$$

Once a crack appears into a specimen, a discontinuity is introduced. Therefore, with the lack of a continuous structure it is difficult to compare with a plain and monolithic structure such as that submitted to pre-crack. With that in mind, it seems more coherent to compare just the part of the graph inherent to the fibers domain, such as the post cracking branch. In order to do that, the energy of each curve post first crack was calculated on Grapher Software. Therefore, besides the aforementioned indexes, the performance of the healed and control specimens was also assessed by calculating the post-cracking energy, as the area subtended by the stress vs COD curve, starting from the first crack and up to a 0.8 mm of displacement, as shown in Figure 3 (b).

2.5. Computer Tomography Scan (CT Scan)

In order to determine the fiber distribution and orientation in the slab as cast, CT Scan was performed for a few chosen samples after the final direct tensile tests. The scans were performed in a vtomex-m 300 Scan from Baker Hughes, with 120 kV of tension and electric current of 250uA. The reconstruction was made with Avizo Software with voxel size of 117 µm and no filter was used.

2.6. Composite Fiber dispersion

The steel fiber dispersion at the notched cross-section was also evaluated after the final tensile failure tests through 91 images from each sample acquired with a magnifying glass attached to a microscope. After that, a mosaic of the acquired images was constructed and the steel fibers were counted with support of Fiji software. Finally, the results were analyzed with a proper code written on MatLab.

Figure 4 shows section A-A and the cross-section XY divided into three regions along the Y axis (R1, R2 and R3), in which R1 is closer to the slab top and R3 to the slab bottom. In order to calculate the density, the amount of steel fibers in each region was divided by the total amount of steel fibers in the cross-section.

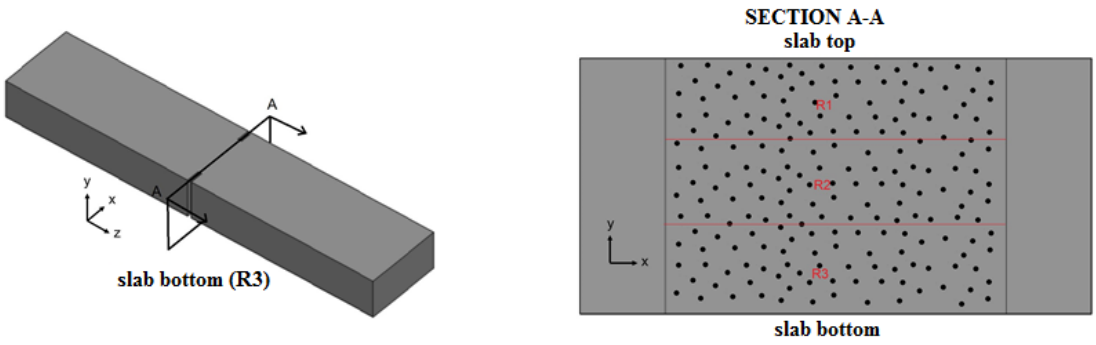

(a) (b)

Figure 4. Illustration of fiber dispersion analysis: tensile test sample (a) sample cross section (Section A-A); (b) idealization of a uniform fiber dispersion in the sample cross section

2.7. Thermogravimetric analysis

Thermogravimetric analysis was performed on two different samples; one from a cast paste containing slag+cement and another one from the "white" material extracted from inside the healed crack.

The first one was performed in order to investigate the role of slag in the self-healing of the matrix and the second in order to characterize the material which fills the crack. The test was performed in a thermo-balance TGA/DTG/DSC simultaneous, model SDT Q600 manufactured by TA Instruments, using crushed and dried material spread uniformly on the aluminum crucible. The pyrolysis process was performed at heating rates of 10°C/min in a nitrogen flow of 100 ml/min and the temperature of the furnace was programmed to rise from 25º to 1000°C. The samples were crushed with a pestle and then sifted in a 150 µm mesh. The hydration was stopped in the paste material that passed through the mesh with isopropyl alcohol during 3 days.

3. RESULTS AND DISCUSSION

3.1. Crack opening, steel fiber alignment and distribution

Figure 5 shows the crack opening pattern observed in all specimens submitted to crack induction tests. The crack opening features a 3D patterns, being larger in R1 regions (close to the free cast surface) and narrower in R3 regions, close to the mould-bottom.

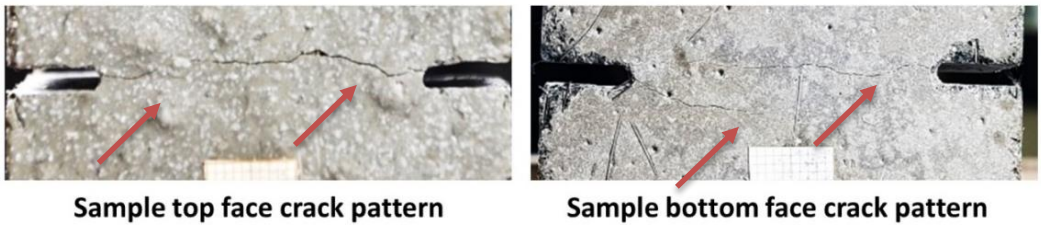

Figure 5. Typical tensile crack pattern of top and bottom of specimens

Figure 6 shows the typical result obtained through a longitudinal cut of the thickness, Z axis, on R1, R2 and R3 by. The first frame (a.1, b.1, c.1) shows the cutting plane and the second (a.2, b.2, c.2) shows the XZ plane (longitudinal cut). According to CT Scan analysis, the steel fibers distribution on the specimen's longitudinal cut is different. It is possible to see that the number of fibers on Region 1 is considerably lower in comparison to Region 2 and 3. This was observed in all studied specimens. It is also possible to observe a higher apparent porosity, by the high number of pores in Region 1. It is possible to conclude that a fiber settlement occurred at the bottom of the slab. Similar results have been published by Ferrara et al [20], concluding that even in a mix with suitably adapted rheology and carefully controlled mixing and casting procedures this difference is almost unavoidable.

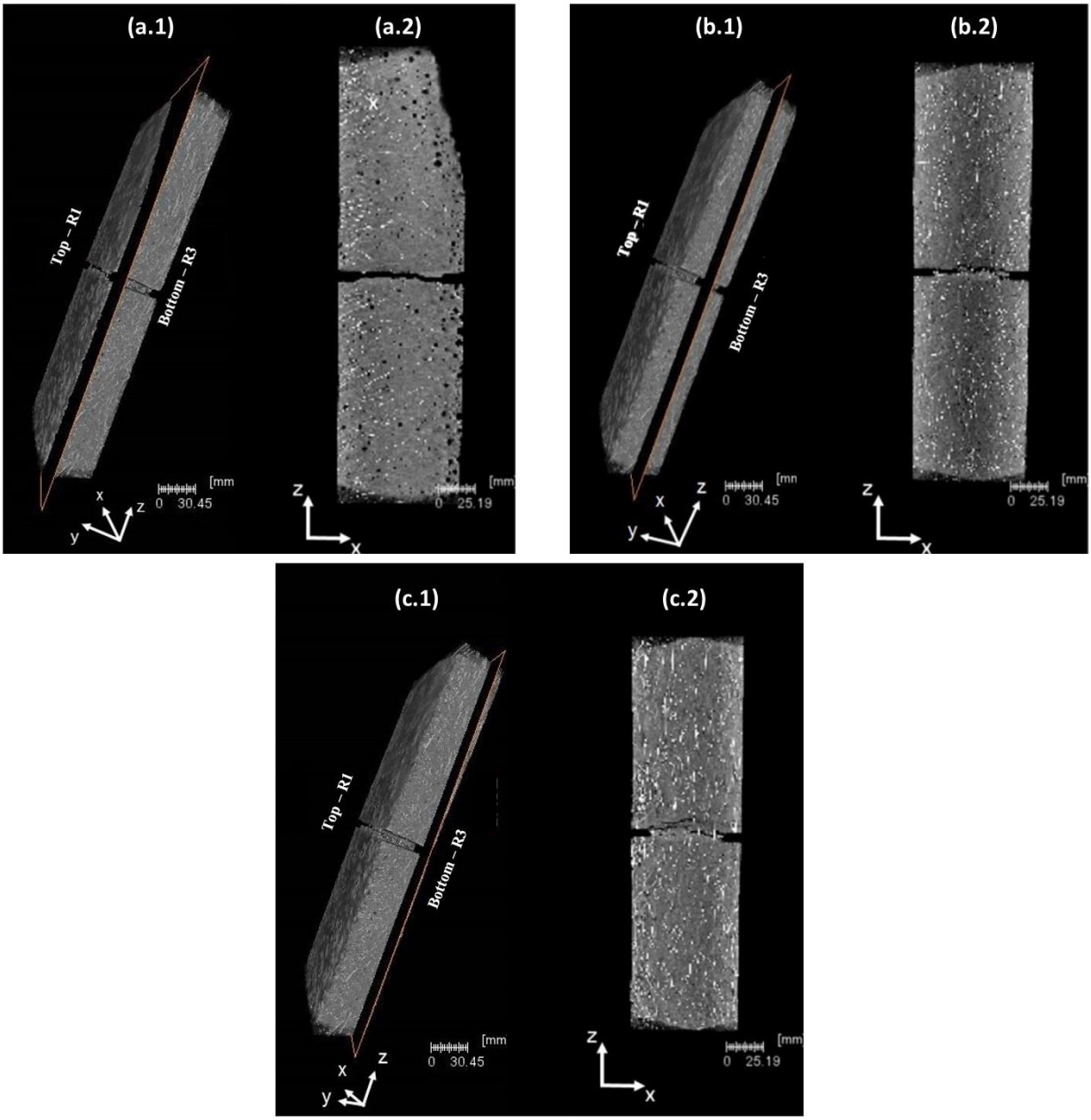

Figure 6. CT Scan of typical specimen showing three different sections: (a.1) R1 (top of the slab) cutting section (a.2) ZX axis of R1 section; (b.1) Middle of the slab section (b.2) ZX axis of b.1 section; (c.1) R3 (bottom of the slab) section (c.2) ZX axis of R3 section

For both studied mix designs, Region 1, 2 and 3 (respectively from top to bottom of the slab) present an average fiber amount respectively equal to 25, 35 and 40% of the total (see Table 3 and Figure 7). The lower number of fibers at the top surface of specimens generates a weaker zone, responsible of a higher crack opening at this region. Due to these differences on crack opening at each region, the observed crack has a trapezoidal pattern.

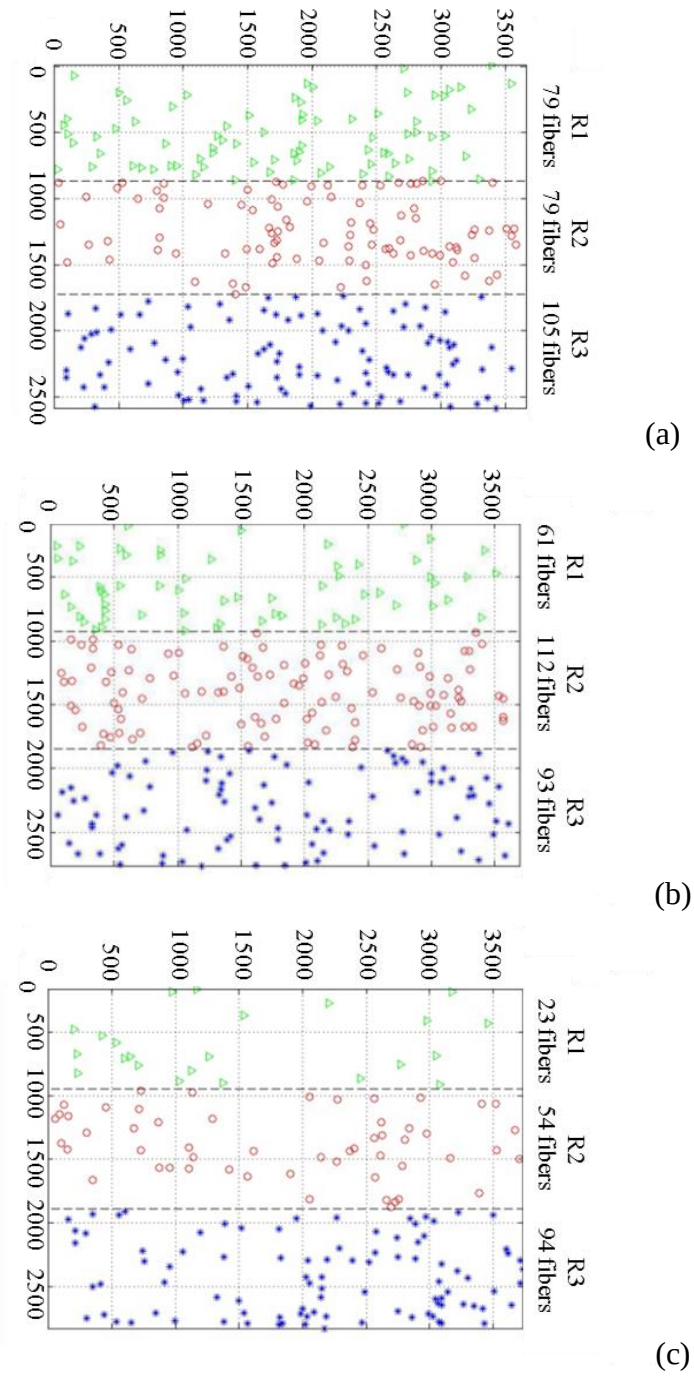

Figure 7. Fiber density calculated on the cross section XY of each specimen respectively (a) A26, (b) B26 and (c) C26

Table 3
Composite Fiber dispersion of S1.28 and S1.28S_i0.28 slab samples at different locations

Slab location	S1.28			S1,28Si0,28		
	R1	R2	R3	R1	R2	R3
A	25±3%	34±2%	41±3%	25±3%	33±4%	42±4%
B	25±4%	35±4%	40±5%	24±1%	34±3%	42±3%
C	25±1%	35±3%	40±5%	25±3%	35±4%	40±2%
Total	25±3%	35±3%	40±4%	24±2%	33±4%	41±4%

As described in section 2.2, the casting procedure was conceived in order to allow fiber alignment parallel to concrete flow, which results, along that same direction, into enhanced crack control ability and hence increased mechanical performance [8] [11] [20] . A concrete flow from Location A to C and from the center of slab to the sides was observed. In order to prove that a random choice of specimen was effective, the total fiber content of all specimens from Location A, Location B and Location C were taken into account. The average amount of fiber on Location A, B and C for mix designs S1.28Si0.28 was 34±2%, 33±1% and 34±1%, respectively and for mix design S1.28 was 32±3%, 34±3% and 34±2%, respectively for Location A, B and C. This confirms that for both investigated composites homogeneous fiber dispersion throughout the slab was achieved.

3.2. Crack induction and Self-healing evaluation

The results of mechanical tests are presented in Figure 8. For both studied cases, gray curves indicate the phase 1 (pre-crack), followed by black curves (tensile test after treatment) and orange curves (non-precracked samples/control). Composites with steel fibers only (see Figure 8(a)) presents an average value of first crack stress at crack induction equal to 5,48±0,64 MPa and maximum tensile stress equal to 6.91±0,90 MPa, with an average stiffness of 47±4 GPa. The use of sisal fibers promoted an increase on such properties (Figure 8(b)). The average of first crack stress for crack induction was 5,75±0,16 MPa, maximum tensile average equal to 9.20±0.74 MPa and an average stiffness of 52±1 GPa was calculated.

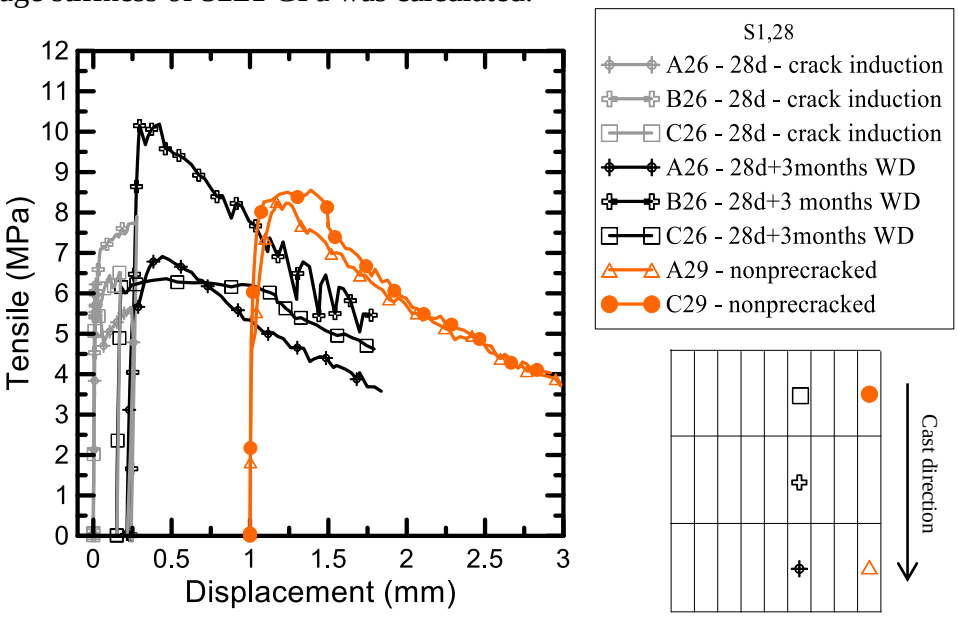

(a)

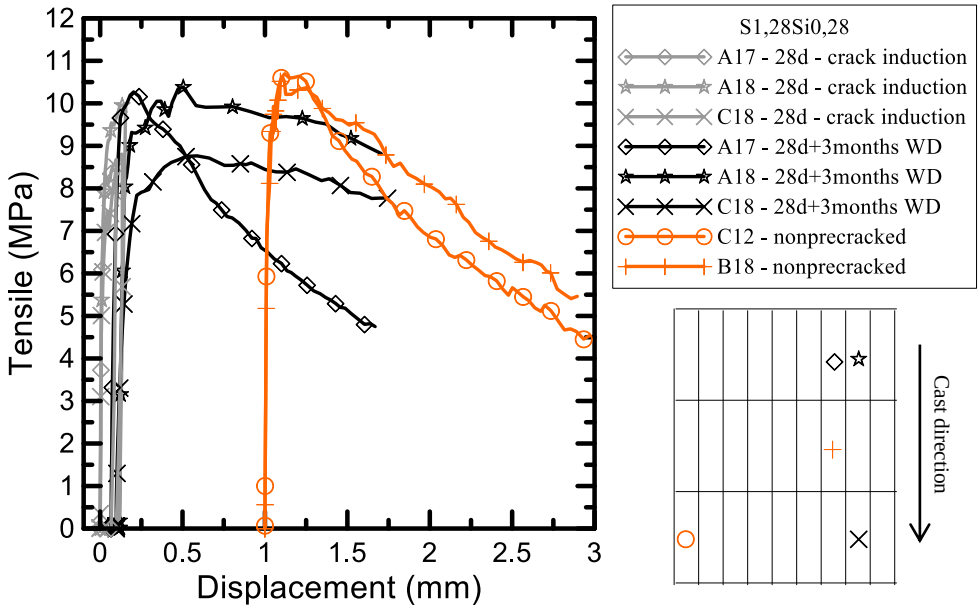

(b)

Figure 8. Results of stress x displacement curves for steel fibers crack induction (gray) and after 3 months of wet and dry cycles (black) and control samples (orange) (a) S1,28 (b) S1,28Si0.28

In all studied cases it was clearly observed a typical strain-hardening behavior, characterized by an increase of stress after first cracking and multiple crack patterns (see, e.g. Figure 9 and 10).

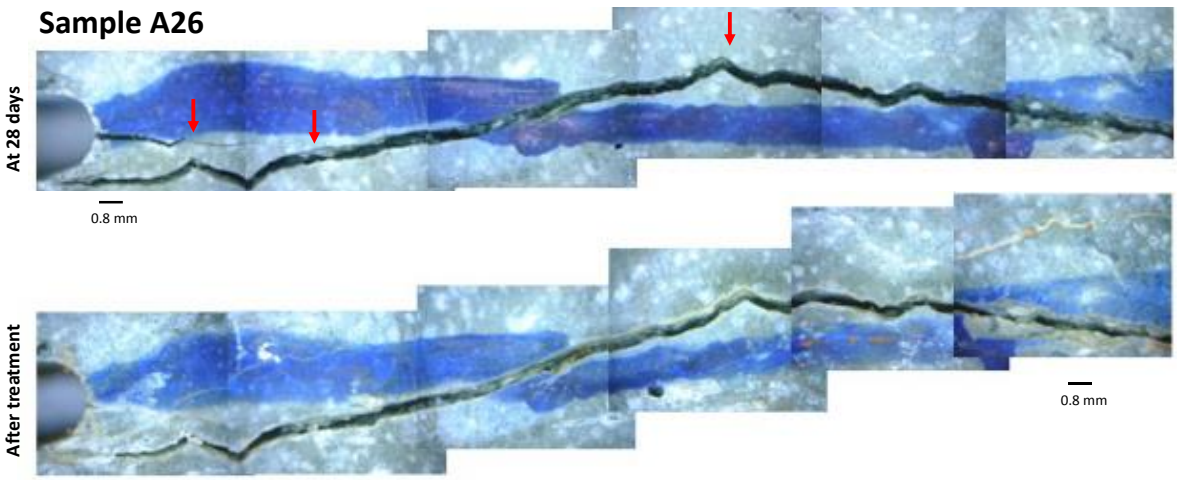

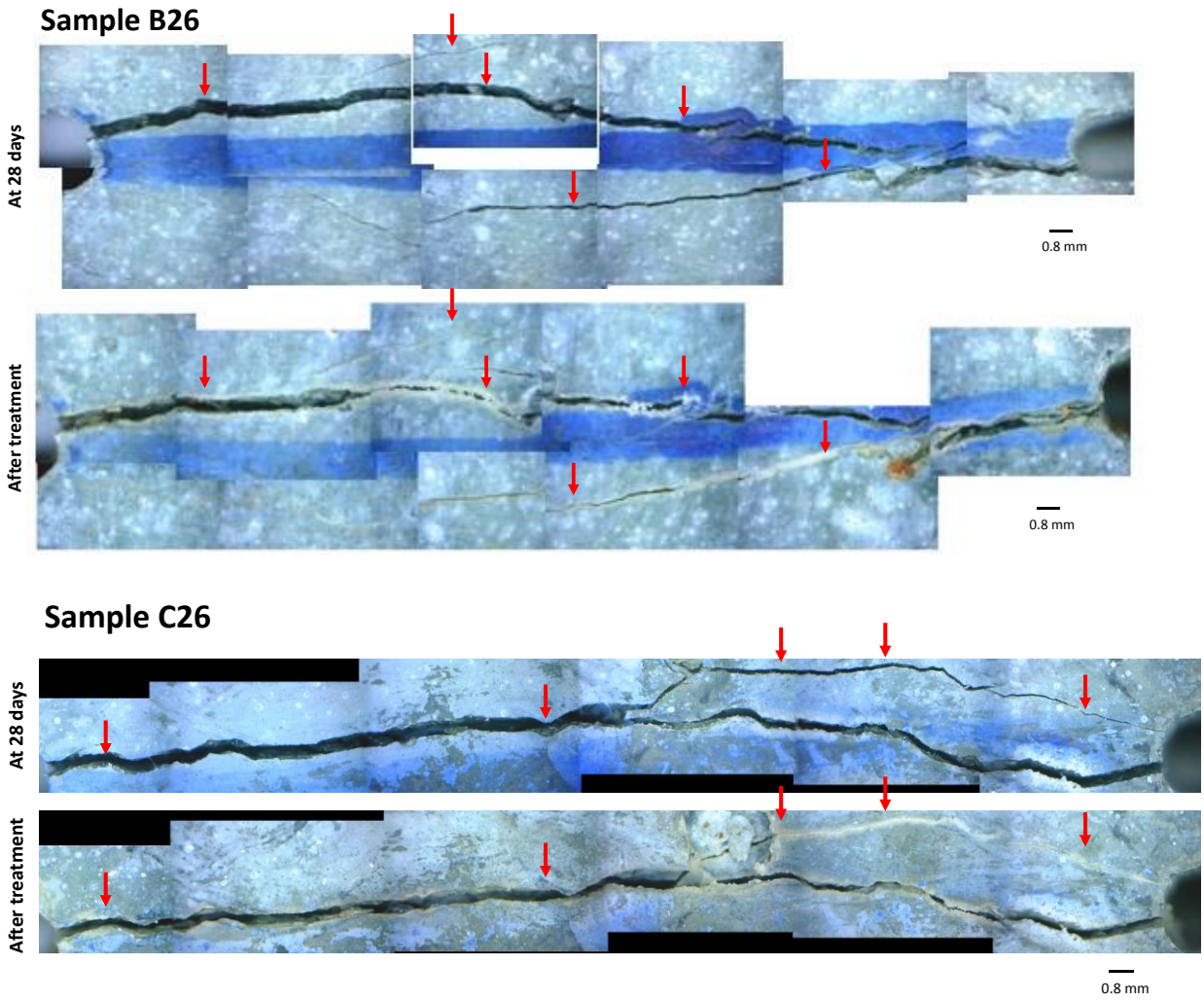

Figure 9. Mosaic images of cracks pattern of tensile test samples from S1.28 at 28 days age and after treatment (after 3 months of wet and dry cycles). Red arrows indicate sealing areas with calcium hydroxide.

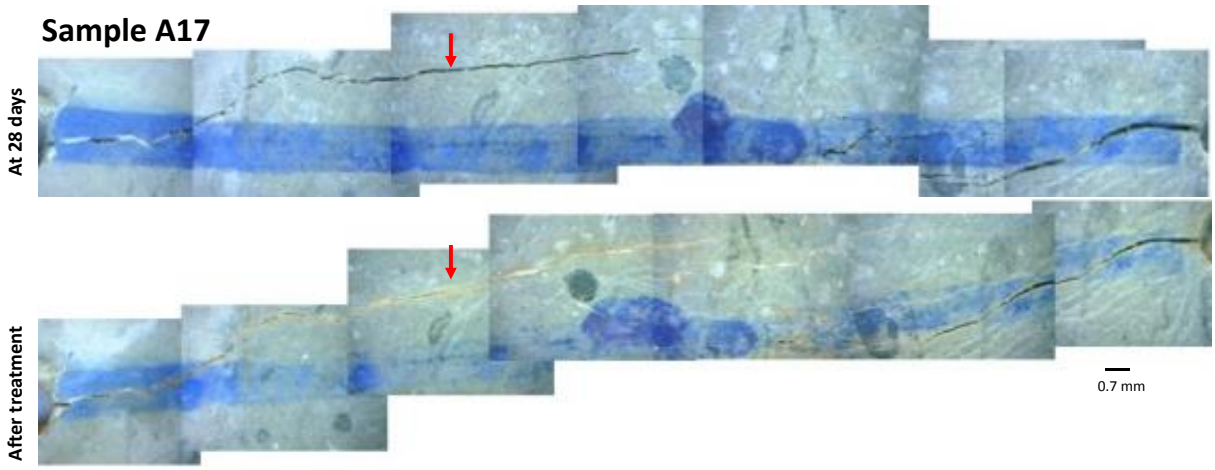

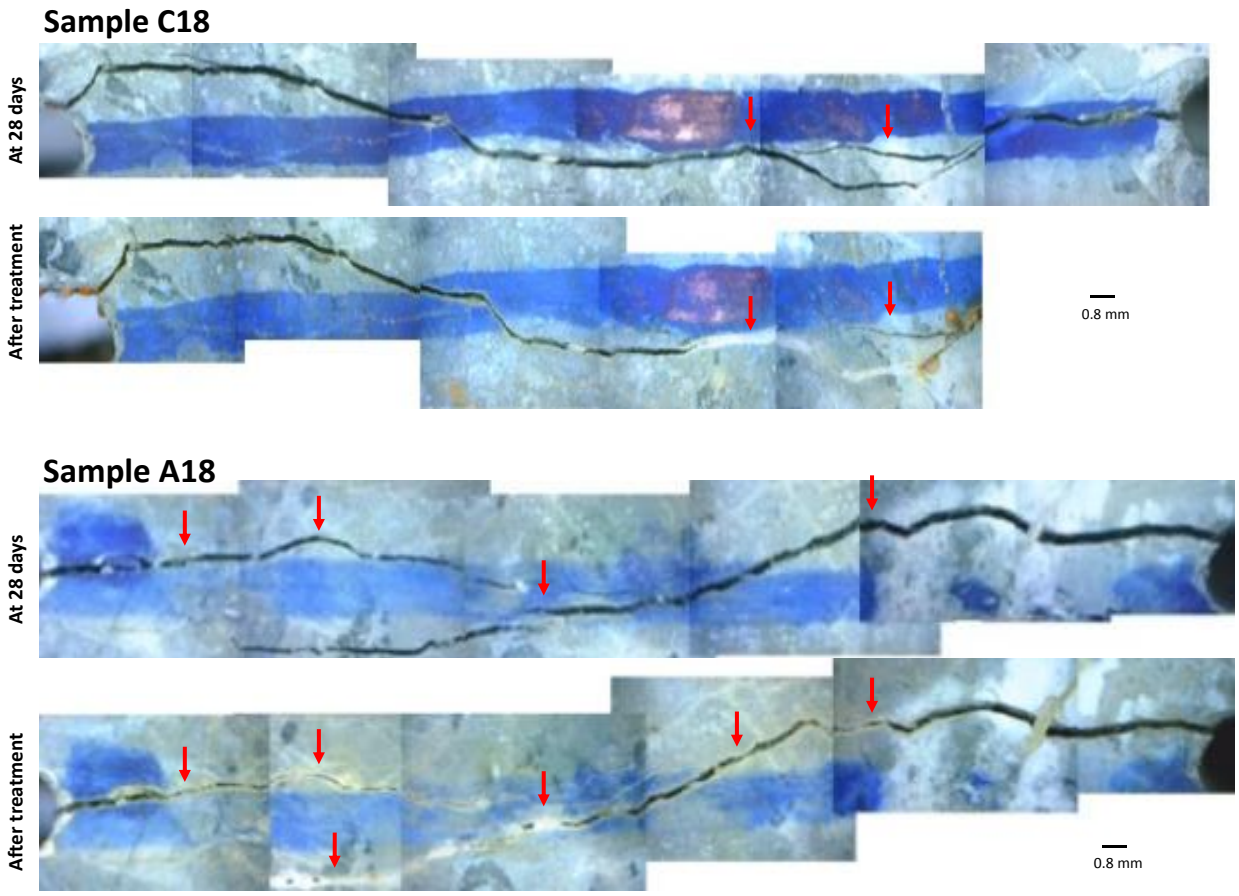

Figure 10. Mosaic images of cracks pattern of tensile test samples from S1.28Si0.28 at 28 days age and after treatment (after 3 months of wet and dry cycles). Red arrows indicate sealing areas with calcium carbonate.

After 3 months of treatment the pre-cracked specimens were resubmitted to tensile test, together with control companion specimens, which underwent the same wetting and drying cycle exposure. The curves from specimens cast with the mix with only steel fibers highlight an average tensile strength equal to 7.89±2.16 MPa, higher than the tensile stress at 28 days for all studied specimens, with a stiffness of 24±5 GPa. Observing the initial slope of the black curves it is possible to see the recovery in strength and stiffness that can be reasonably attributed to both crack closure and fiber matrix interface densification [26]. Regarding the samples with sisal fibers addition, they presented an average tensile stress of 9.84±0.88 MPa, also higher than the value at 28 days, and stiffness equal to 28±4 GPa. It is possible to compare the stiffness from unloading branch of pre-crack curves (gray) with the stiffness from specimens with 3 months of wet and dry cycles (black curves). The mix design with sisal fibers presented an unloading stiffness of 13±1 GPa which correspond to a recovery of 233%. Regarding the steel only mix the unloading stiffness was 9±2 GPa, which correspond to a recovery equal to 267%.

Figure 8(a) and 8(b) also show in orange color, and shifted 1.0 mm along the x axis, the stress-displacement curves of two control specimens. It is possible to see that the control specimens

from steel only mix featured an average tensile strength of 8.49±0.16 MPa, merely 7% higher in comparison to treated samples. Regarding samples with sisal fibers, it is possible to observe an average tensile strength value of 10.81±0.09 MPa, 9% higher in comparison to treated samples. The fact that, despite the not complete closure of the cracks, the load bearing capacity was not compromised, and that healed specimens were able to achieve, after treatment, a tensile strength as high as the companion uncracked specimens undergoing the same curing history, is a clear index of the fact that the measured mechanical performance of the healed specimens, as compared to companion uncracked control ones, is the outcome of concurrent reconstruction of through cracks matrix continuity as well as of the enhancement of fiber-matrix bond through deposition of healing products at the interface.

Figure 9 and 10 show the crack healing on the studied specimens (a) at 28 days and (b) after 3 months of wet and dry cycles, the first one for steel and the second for the steel plus sisal mix. As reported, the crack was composed of a main crack and multiple tiny cracks originating from the main one. It is possible to observe that the phenomenon of self-healing has occurred, sealing completely cracks under 80 μm.

In order to proper evaluate the obtained results, healing indexes were calculated, whose values are presented on Table 4.

Table 4
Healing Indexes and post-crack energy of studied samples

S1.28			
Specimen	ITR_1	ITR_2	IDR
C26	0.97	0.96	0.59
B26	1.31	1.20	0.52
A26	1.23	1.06	0.42
S1.28Si0.28			
Specimen	ITR_1	ITR_2	IDR
A17	1.18	1.16	0.51
C18	1.00	0.94	0.47
A18	1.04	0.97	0.63

It can be observed on ITR1 that specimen B26 and A26 present a recovery index of 131% and 123%, respectively. Specimen C26 recovery 97% of the total tensile load bearing capacity exhibited at crack induction. The same was observed on steel and sisal mix with recovery index varying from 100% to 118%. Even with reference to a more restrictive index, ITR2, that takes into account only the fiber branch behavior, there is evidence of a mechanical recovery. For the steel only mix design, specimens presented a recovery varying from 96% to 120% and the steel plus sisal ones from 94% to 116%. As far as the stiffness is concerned, the specimen did not fully recover to the value of the uncracked specimen, and that can be attributed to the not complete closure of the crack, leading to a discontinuity of the specimen, as already remarked above.

The introduction of a small amount of sisal fibers promoted a positive response of the mechanical performance. Analyzing the results from steel only and steel plus sisal mix designs, the maximum

tensile stress after wetting and drying cycles was 7.89±2,16 MPa and 9.84±0.88 MPa, respectively. It is a difference of almost 2.00 MPa (about 25% if referred to the steel fibers only mix), demonstrating that sisal fibers can play a decisive role in the strength development of the matrix. This could be due to some kind of internal curing (and hence promotion of throughout hydration) due to the fact that sisal fibers carry water through their porous network structure. The integrity of the concrete was also achieved due to calcium carbonate nucleation on these fibers, confirmed by Figure 11, which shows the calcium carbonate on sisal fibers crossing the crack. It is important to highlight that the crack closure (re-integrity) in the samples is a way to protect the concrete reinforcement from oxidation and concrete core from deterioration. Although calcium carbonate crystals have a maximum size of 30 microns, once the sisal fiber work as a nucleation site and a bridge between both faces of the crack it is possible to seal even cracks wider than 30 microns. This nucleation reaction occurs due to the amount of humidity that vegetal fibers contain in their cellular structure. Calcium carbonate is formed by a combination of Ca^{+2}, water and CO_2, dissolved in the former, therefore the humidity inside the fiber is released gradually and in contact with the CO_2 from air and Ca^{+2} from the matrix creating the suitable environment for the formation and of $CaCO_3$ crystals on the fiber.

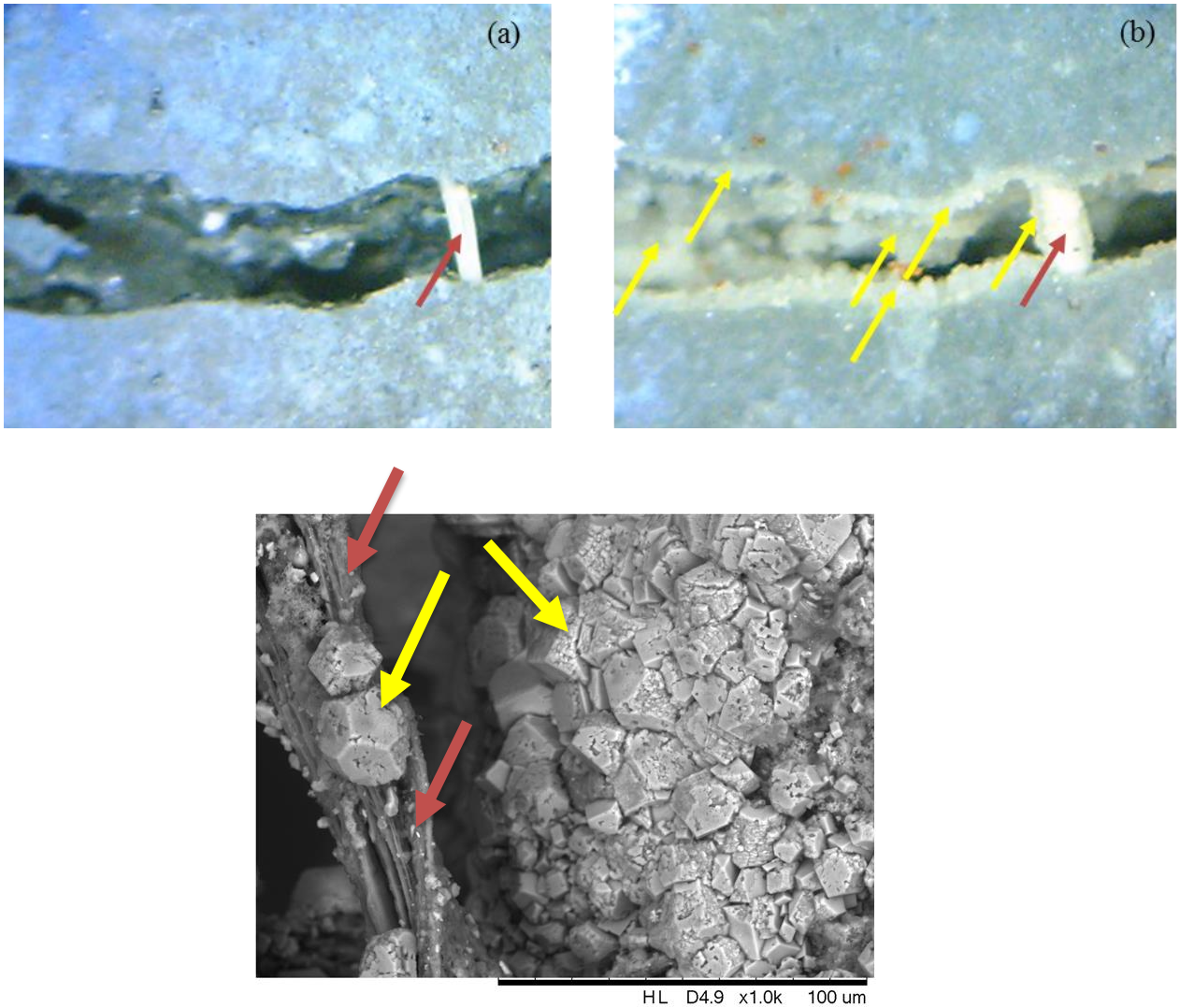

(c)

Figure 11. Nucleation of calcium carbonate on Sisal Fiber [S1,28Si0,28]: (a) at crack induction [28 days]; (b) after wetting and drying cycles [3 months] (c) MEV - calcium carbonate (yellow arrow) on a sisal fiber (red arrow)

3.3. Hydration products formed on the matrix

Through the observation of the crack sealing phenomenon it was possible to see the presence of a white material closing the crack. Therefore a TGA was performed in order to identify the products formed on the matrix. Figure 12 presents the results. The blue line represents the white material mentioned on the previous section. It shows peaks in correspondence of the dehydroxilation of ettringite and C-S-H (until 200°C), CAH and C-A-S-H from the aluminum phase (200-400ºC) and a high peak in correspondence of the decarbonatation (500-750°C). The presence of the aforementioned substances confirms that the products appearing in the cracks are products of the delayed hydration and carbonation reactions, which are the cause of the healing phenomenon during the wet and dry stages. [27] [28]

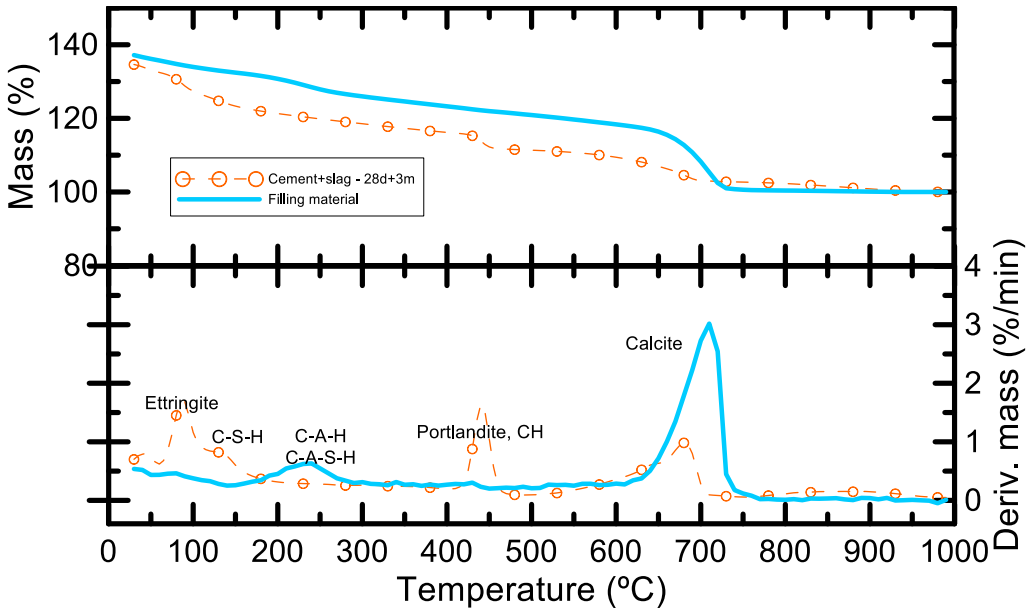

Figure 12. Thermogravimetry results cement paste, cement+slag paste after 3 months of wet and dry cycles, as well the material filling the crack

The dotted line represents a different TGA, as described on section 2.8. The TGA was made from a cement+blast furnace slag paste in order to understand the material formation on the slag-cement matrix. The paste presented a 9.96% water loss from ettringite and C-S-H until 200ºC, followed by a 5.12% mass loss related to the aluminate phase (C-A-H and C-A-S-H) between 200ºC and 400ºC. The paste also presented portlandite dehydroxylation between 400-450ºC at an amount equal to 2.34% of mass. At last occurred 4.8% of CO_2 loss from $CaCO_3$ structure at 500-750ºC. The low amount of $CaCO_3$ can be reasonably attributed to the fact that in the case of the cement+slag paste, since a homogeneous sample with no pre-crack induction was tested, conditions for calcium carbonate to grow were not suitably created.

4. CONCLUSION

In this paper it has been shown that sisal fibers act as facilitators of self-healing phenomenon in UHPFRC cement-slag matrix thanks to their hierarchical microstructure which allows to convey and to distribute water through the bulk matrix and also at the level of fiber-matrix interface. The obtained results allow the following conclusions to be formulated:

1) The proposed mix composition can be identified as a moderated strain hardening UHPFRC, both in the case of sole steel fiber reinforcement or hybrid steel plus sisal fibers one;
2) The applied methodology has been effective in order to provide a controlled crack for self-healing investigation, resulting in a one and only main crack, though with some branching due to the fiber stress redistribution capacity. However, as mentioned, the distribution and orientation of fibers in the slab affected the crack formation, resulting into a three-dimensional features of the crack opening through the thickness of the slabs. This was also confirmed by microscope and CT Scan observations which allowed to quantify the volume of steel fibers and orientation along the length of the slab. The results showed a higher volume fraction of steel fibers at the bottom of the specimen (R3), followed by the central third (R2) and finally the top of the slab (R1).
3) There was a satisfactory healing after 3 months of wetting and drying cycles, especially in the smaller cracks, with openings in the 1-80 μm range. Sisal fibers, added at a 0.28% volume ratio to the mixture with 1,28% by volume of steel fibers, acted as water transport means and also as nucleating agent, accelerating the deposition of calcium carbonate in the crack and also allowing cracks larger than the maximum size of the calcium carbonate crystals to be sealed. Thanks to the water transport function played by sisal fibers, the healing kinetic was faster in the mix with hybrid fiber reinforcement, also promoting a higher mechanical performance than in the mix with only steel fibers.
4) The self-healing phenomenon that resulted in the healing of the cracks is related to late hydration of cement/slag matrix products, as confirmed by the presence of calcium carbonate, C-A-S-H and C-A-H. These phases were presented both in a reference matrix paste as well as in the crack filling material, though in the latter higher calcium carbonate content was presented, thanks to the conditions for its formation created rightly by the crack formation and the presence of through crack sisal fibers.
5) Indexes defined and calculated for the quantification of self-healing phenomenon denoted a capacity of the material to retain its pristine mechanical performance, upon cracking and successive healing, even under not complete sealing/closure of the cracks. This may indicate a role, in the overall assessment of the healing induced recovery/retentions of the mechanical performance, not only by the reconstruction of the through crack matrix continuity but also by the densification of fiber-matrix interface as well as of the healing of cracks created upon fiber pull-out at the fiber-matrix interface.

5. REFERENCE

1) Han, B., Yu, X., Ou, J., Han, B., Yu, X., & Ou, J. (2014). Challenges of self-sensing concrete. *Self-Sensing Concrete in Smart Structures. Oxford, UK: Butterworth Heinemann*, 361-376.
2) Özbay, E.,Sahmaran, M., Yücel, H. E., Erdem, T. K., Lachemi, M., & Li, V. C. (2013). Effect of sustained flexural loading on self-healing of engineered cementitious composites. Journal of

Advanced Concrete Technology, 11(5), 167-179.
3) Zhang, W., Zheng, Q., Ashour, A., & Han, B. (2020). Self-healing cement concrete composites for resilient infrastructures: A review. Composites Part B: Engineering, 189, 107892.
4) De Belie, N., Gruyaert, E., Al-Tabbaa, A., Antonaci, P., Baera, C., Bajare, D. & Litina, C. (2018). A review of self-healing concrete for damage management of structures. Advanced materials interfaces, 5(17), 1800074.
5) Rock, M. L., Tranchitella, L. J., & Pilato, R. S. (1997). Control of calcium carbonate particle size and shape by precipitation from CTAB/alcohol/hexadecane mixtures. Colloid and Polymer Science, 275(9), 893-896.
6) Martín-Martínez, M. J. (2002). Rubber base adhesives. Adhesion Science and Engineering, 573–675.
7) Krelani, V. (2015). Self-healing capacity of cementitious composites. PhD Thesis, Politecnico di Milano.
8) Ferrara, L., Krelani, V., Moretti, F., Flores, M. R., & Ros, P. S. (2017). Effects of autogenous healing on the recovery of mechanical performance of High Performance Fibre Reinforced Cementitious Composites (HPFRCCs): Part 1. Cement and Concrete Composites, 83, 76-100.
9) Mehta, P. K., & Monteiro, P. J. (2014). Concrete: microstructure, properties, and materials. McGraw-Hill Education.
10) de Souza Oliveira, A., Gomes, O. D. F. M., Ferrara, L., Fairbairn, E. D. M. R., & Toledo Filho, R. D. (2021). An overview of a twofold effect of crystalline admixtures in cement-based materials: From permeability-reducers to self-healing stimulators. Journal of Building Engineering, 102400.
11) Ferrara, L., Krelani, V., & Carsana, M. (2014). A "fracture testing" based approach to assess crack healing of concrete with and without crystalline admixtures. Construction and Building Materials, 68, 535-551.
12) Cuenca, E., Tejedor, A., & Ferrara, L. (2018). A methodology to assess crack-sealing effectiveness of crystalline admixtures under repeated cracking-healing cycles. Construction and Building Materials, 179, 619-632.
13) Blaiszik, B. J., Kramer, S. L., Olugebefola, S. C., Moore, J. S., Sottos, N. R., & White, S. R. (2010). Self-healing polymers and composites. Annual Review of Materials Research, 40, 179-211.
14) De Belie, N., & De Muynck, W. (2008). Crack repair in concrete using biodeposition. In Proceedings of the International Conference on Concrete Repair, Rehabilitation and Retrofitting (ICCRRR), Cape Town, South Africa (pp. 291-292).
15) Yang, Y., Lepech, M. D., Yang, E. H., & Li, V. C. (2009). Autogenous healing of engineered cementitious composites under wet–dry cycles. Cement and Concrete Research, 39(5), 382-390.
16) Ferrara, L., Van Mullem, T., Alonso, M. C., Antonaci, P., Borg, R. P., Cuenca, E., & De Belie, N. (2018). Experimental characterization of the self-healing capacity of cement based materials and its effects on the material performance: A state of the art report by COST Action SARCOS WG2. Construction and Building Materials, 167, 115-142.
17) Snoeck, D., Van Tittelboom, K., Steuperaert, S., Dubruel, P., & De Belie, N. (2014). Self-healing cementitious materials by the combination of microfibres and superabsorbent polymers. Journal of Intelligent Material Systems and Structures, 25(1), 13-24.
18) Gupta, S., Al-Obaidi, S. and Ferrara, L.: "Meta-analysis and Machine Learning Models to Optimize the Efficiency of Self-Healing Capacity of Cementitious Material", *submitted for publication to MPDI Materials, June 30th 2021.*
19) di Summa, D., Snoeck, D., Tenório Filho, J.R., Van den Heede, P., Van Vlierberghe, S., De

Belie,N. and Ferrara, L. (2021): Sustainability and economic viability of self-healing concrete containing SuperAbsorbent polymers submitted to RILEM 75th week conference, Merida, Mexico.

20) Ferrara, L., Ozyurt, N., & Di Prisco, M. (2011). High mechanical performance of fibre reinforced cementitious composites: the role of "casting-flow induced" fibre orientation. Materials and Structures, 44(1), 109-128.

21) Monte, F. L., & Ferrara, L. (2021). Self-healing characterization of UHPFRCC with crystalline admixture: Experimental assessment via multi-test/multi-parameter approach. Construction and Building Materials, 283, 122579.

22) Fidelis, M. E. A., Pereira, T. V. C., Gomes, O. D. F. M., de Andrade Silva, F., & Toledo Filho, R. D. (2013). The effect of fiber morphology on the tensile strength of natural fibers. *Journal of Materials Research and Technology*, *2*(2), 149-157.

23) Ferreira, S. R., Lima, P. R. L., Silva, F. A., & Toledo Filho, R. D. (2014). Effect of sisal fiber hornification on the fiber-matrix bonding characteristics and bending behavior of cement based composites. In Key Engineering Materials (Vol. 600, pp. 421-432). Trans Tech Publications Ltd.

24) Hill, C. A., Norton, A., & Newman, G. (2009). The water vapor sorption behavior of natural fibers. Journal of Applied Polymer Science, 112(3), 1524-1537.

25) Espert, A., Vilaplana, F., & Karlsson, S. (2004). Comparison of water absorption in natural cellulosic fibres from wood and one-year crops in polypropylene composites and its influence on their mechanical properties. Composites Part A: Applied science and manufacturing, 35(11), 1267-1276.

26) Qiu, J., He, S., Wang, Q., Su, H., Yang, E.H. (2019). Autogenous healing of fibre/matrix interface and its enhancement. Proceedings 10th International Conference on Fracture Mechanics of Concrete and Concrete Structures FraMCoS-X G. Pijaudier-Cabot et al. (Eds). Bayonne 23-26.

27) Dweck, J., Melchert, M. B. M., Cartledge, F. K., Leonardo, R. S., & Toledo Filho, R. D. (2017). A comparative study of hydration kinetics of different cements by thermogravimetry on calcined mass basis. Journal of Thermal Analysis and Calorimetry, 128(3), 1335-1342.

28) Dweck, J., Buchler, P. M., Coelho, A. C. V., & Cartledge, F. K. (1999). Controle de qualidade de cimento Portland composto por termogravimetria. In Anais do 43o Congresso Brasileiro de Cerâmica, SC (pp. 37-901).

Conflict of Interest (Please upload in Word format)

Declaration of interests

☐The authors declare that they have no known competing financial interests or personal relationships that could have appeared to influence the work reported in this paper.

☒The authors declare the following financial interests/personal relationships which may be considered as potential competing interests:

Tamara Nunes da Cunha Moreira reports financial support was provided by Coordination of Higher Education Personnel Improvement.